Optics Letters

# Accurate optoelectronic third-order nonlinearity characterization using improved carrier-shifted phase modulation

Kunqian Yang,[1] Yuqing Heng,[1] Yunqi Liao,[1] Xingbang Zhu,[1] Jianbin Fu,[2] Min Xue,[1,*] and Shilong Pan[1]

[1] National Key Laboratory of Microwave Photonics, Nanjing University of Aeronautics and Astronautics, Nanjing 210016, China
[2] Newkey Photonics Information Technology Limited Liability Company, Nanjing 210016, China
*xuemin@nuaa.edu.cn

Received 15 May 2026; revised 14 June 2026; accepted 28 June 2026; posted 29 June 2026; published 14 July 2026

**We propose and demonstrate an optoelectronic method for accurately characterizing the third-order nonlinearity of photodetectors (PDs) using improved carrier-shifted phase modulation. A carrier-shifted phase-modulated probe signal is injected into the PD under test, and the third-order nonlinear characteristics are extracted by measuring the powers of the fundamental and third-order intermodulation distortion (IMD3) components as the probe signal power is swept. To enhance measurement accuracy, a continuous-wave laser is employed for power compensation, maintaining a constant operating condition for the PD throughout the sweep. Moreover, an additional optical frequency shifter is inserted before the phase modulator (PM) to reduce the frequency spacing between the fundamental components, and a de-embedding procedure is employed to remove the contribution of the PM's nonlinearity. Experimentally, the spur-free dynamic ranges (SFDRs) of a commercial PD are measured over 10–67 GHz, and the effects of frequency spacing and input power on measurement accuracy are investigated.** 

https://doi.org/10.1364/OL.604680

Photodetectors (PDs) are key devices for optical-to-electrical (O/E) conversion in modern photonic systems, and they are widely used in high-speed optical communications [1], optical fiber sensing [2], and microwave photonics [3]. Conventionally, a PD's performance is characterized by its small-signal frequency response, which indicates both the working bandwidth and conversion efficiency [4]. Nonetheless, O/E conversion is inherently nonlinear. In applications such as coherent optical networks and ultra-linear analog radio-over-fiber links, where PDs often operate at high optical power, this nonlinearity can significantly degrade system performance [5,6]. As a result, accurate characterization of a PD's nonlinear parameters is essential.

Among nonlinear parameters, third-order intermodulation distortion (IMD3) is particularly important because it enables the extraction of the third-order intercept point (IP3) and spur-free dynamic range (SFDR). Improved optical heterodyne methods are widely regarded as highly accurate for the IMD3 characterization [7,8]. In these methods, an additional laser pair is introduced into a conventional optical heterodyne scheme to generate two-tone photocurrents. However, these approaches require stable phase and frequency relationships among multiple lasers and therefore rely on wide-bandwidth phase-locked loops (PLLs), which increase system complexity and impose bandwidth limitations. To avoid PLLs, the parallel O/E modulation methods have been proposed [9–11], in which closely spaced RF tones are modulated onto separate optical carriers to generate independent optical double-sideband (ODSB) signals that are combined and detected to produce the desired two-tone photocurrent. Although three-tone schemes and de-embedding techniques can reduce modulator-induced distortion [10,11], these methods still require multiple lasers and electro-optic modulators (EOMs) operated at the quadrature transmission point, leading to substantial experimental complexity and limited stability. Recently, an optical heterodyne method based on carrier-shifted phase modulation was demonstrated [12]. In that scheme, two optical carriers derived from the same laser are frequency shifted and phase modulated separately, and the beat notes between the shifted carrier and the ±1st-order sidebands are used as the fundamental components. Because it uses a single laser and RF source and avoids EOM bias drift, it offers a simpler and more stable platform for PD nonlinearity measurement. Nevertheless, the large and fixed two-tone spacing may become less favorable when the PD frequency response is not sufficiently flat, and the varying operating point during RF power sweeping may affect the stability of nonlinear characterization.

In this Letter, we propose and experimentally demonstrate an optoelectronic method for accurately characterizing the third-order nonlinearity of PDs using improved carrier-shifted phase modulation. The proposed method adopts optical power compensation to keep the PD under a stable operating condition during the probe signal power sweeping, which is essential for reliable IMD3 characterization. To further enhance accuracy, a supplementary optical frequency shifter is introduced to reduce the frequency spacing between the generated two-tone components. Additionally, the influence of the phase modulator (PM)'s

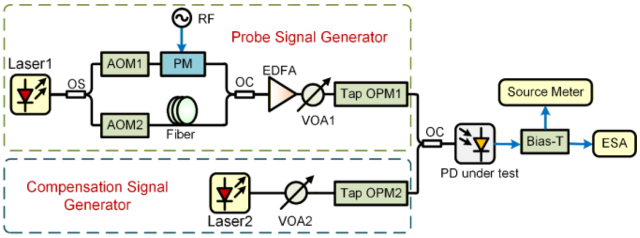


**Fig. 1.** The schematic of the proposed measurement method. AOM, acousto-optic modulator; EDFA, erbium-doped fiber amplifier; ESA, electrical spectrum analyzer; OC, optical coupler; OS, optical splitter; PD, photodetector; PM, phase modulator; Tap OPM, tap optical power meter; VOA, variable optical attenuator.

nonlinearity is removed through a de-embedding process. By the proposed approach, the SFDR of a commercial wideband PD is characterized over the 10–67 GHz, and the effects of two-tone frequency spacing and optical input power on the measurement results are experimentally investigated.

Figure 1 shows the schematic of the proposed measurement method. The phase-modulated optical signal generated in the upper arm and the frequency-shifted carrier from the lower arm are combined to form a carrier-shifted phase-modulated probe signal, which can be expressed as:

$$\begin{aligned} E_{\mathrm{p}}(t) =& E_{\mathrm{c}} \exp\left[j2\pi\left(f_{\mathrm{c}}+f_{\mathrm{s1}}\right)t + j\beta\sin\left(2\pi f_{\mathrm{e}}t\right)\right] \\ &+ E_{\mathrm{sc}}\exp\left[j2\pi\left(f_{\mathrm{c}}+f_{\mathrm{s2}}\right)t\right] \end{aligned}, \tag{1}$$

where $E_{\mathrm{c}}$ and $f_{\mathrm{c}}$ are the amplitude and frequency of the optical carrier at the PM input, $\beta$ is the modulation index, $f_{\mathrm{s1}}$ and $f_{\mathrm{s2}}$ are respectively the frequency shifts introduced by acousto-optic modulators (AOMs), $f_{\mathrm{e}}$ is the RF drive frequency, and $E_{\mathrm{sc}}$ is the amplitude of the frequency-shifted carrier. The optical intensity of the probe signal can be expressed as:

$$\begin{aligned} \left|E_{\mathrm{p}}(t)\right|^2 &= E_{\mathrm{c}}^2 + E_{\mathrm{sc}}^2 + 2E_{\mathrm{c}}E_{\mathrm{sc}}\cos\left[\beta\sin\left(2\pi f_{\mathrm{e}}t\right) - \Delta ft\right] \\ &= E_{\mathrm{c}}^2 + E_{\mathrm{sc}}^2 + 2E_{\mathrm{c}}E_{\mathrm{sc}}\sum_{n=-\infty}^{+\infty} J_n(\beta)\cos\left[2\pi\left(nf_{\mathrm{e}}-\Delta f\right)t\right], \end{aligned} \tag{2}$$

where $\Delta f = f_{s2} - f_{s1}$, and $J_n(\cdot)$ is the $n$th-order Bessel function of the first kind. An erbium-doped fiber amplifier (EDFA) followed by a variable optical attenuator (VOA) is used for probe power sweeping, while a second laser provides power compensation to maintain a constant DC photocurrent and thereby stabilize the operating condition of the PD under test. As the carrier spacing between the two lasers is far beyond the PD bandwidth, the beat note between them has no influence on the measurement. Accordingly, the AC photocurrent generated by the PD under test can be written as:

$$\begin{aligned} i_{\mathrm{AC}}(t) &= \eta(f)\left|E_{\mathrm{p}}(t)\right|^2 \\ &= \eta(f)\, 2E_{\mathrm{c}}E_{\mathrm{sc}}\sum_{n=-\infty}^{+\infty} J_n(\beta)\cos\left[2\pi\left(nf_{\mathrm{e}}-\Delta f\right)t\right], \end{aligned} \tag{3}$$

where $\eta(f)$ is the frequency-dependent responsivity of the PD under test. At high optical power, the nonlinear responsivity of the PD can be represented by a Taylor expansion as [13]:

$$i(t) = \alpha_0 + \alpha_1 i_{\mathrm{AC}}(t) + \alpha_2\left[i_{\mathrm{AC}}(t)\right]^2 + \alpha_3\left[i_{\mathrm{AC}}(t)\right]^3 + \cdots, \tag{4}$$

where $\alpha_k$ is the $k$th-order nonlinear coefficient. The quadratic terms in Eq. (4) are given by:

$$\begin{aligned} \alpha_2\left[i_{\mathrm{AC}}(t)\right]^2 = 2\alpha_2 E_{\mathrm{c}}^2E_{\mathrm{sc}}^2 &\sum_{n=-\infty}^{+\infty}\sum_{p=-\infty}^{+\infty} J_n(\beta)J_p(\beta)\cdot \\ &\{\cos\left[2\pi\left((n+p)f_{\mathrm{e}}-2\Delta f\right)t\right] \\ &+\cos\left[2\pi\left(n-p\right)f_{\mathrm{e}}t\right]\}. \end{aligned} \tag{5}$$

And the cubic terms in Eq. (4) are given by:

$$\begin{aligned} \alpha_3\left[i_{\mathrm{AC}}(t)\right]^3 = 2\alpha_3E_{\mathrm{c}}^3E_{\mathrm{sc}}^3 &\sum_{n=-\infty}^{+\infty}\sum_{p=-\infty}^{+\infty}\sum_{q=-\infty}^{+\infty} J_n(\beta)J_p(\beta)J_q(\beta)\cdot \\ &\{\cos\left[2\pi\left((n+p+q)f_{\mathrm{e}}-3\Delta f\right)t\right] \\ &+\cos\left[2\pi\left((n+p-q)f_{\mathrm{e}}-\Delta f\right)t\right] \\ &+\cos\left[2\pi\left((n-p+q)f_{\mathrm{e}}-\Delta f\right)t\right] \\ &+\cos\left[2\pi\left((n-p-q)f_{\mathrm{e}}+\Delta f\right)t\right]\}. \end{aligned} \tag{6}$$

Beating between the ±1st-order sidebands and the frequency-shifted carrier generates the two fundamental components at $f_1 = f_{\mathrm{e}} - \Delta f$ and $f_2 = f_{\mathrm{e}} + \Delta f$. For $n+p+q = 1$ and $n, p, q = \pm 1$, the intrinsic third-order nonlinearity of the PD then produces IMD3 components at $f_{\mathrm{e}} - 3\Delta f$ and $f_{\mathrm{e}} + 3\Delta f$, as described by:

$$\begin{aligned} i_{\mathrm{P}}(t) &= 2\alpha_3E_{\mathrm{c}}^3E_{\mathrm{sc}}^3\sum_{n=-\infty}^{+\infty}\sum_{p=-\infty}^{+\infty}\sum_{q=-\infty}^{+\infty} J_n(\beta)J_p(\beta)J_q(\beta) \\ &\quad\{\cos\left[2\pi\left((n+p+q)f_{\mathrm{e}}-3\Delta f\right)t\right]\} \\ &= -6\alpha_3E_{\mathrm{c}}^3E_{\mathrm{sc}}^3J_1^3(\beta)\cos\left[2\pi\left(f_{\mathrm{e}}-3\Delta f\right)t\right]. \end{aligned} \tag{7}$$

When the PM-induced higher-order sidebands are taken into account, the IMD3 terms satisfying $n+p+q = 1$ are expressed as:

$$\begin{aligned} i_{\mathrm{D}}(t) &= 2\alpha_3E_{\mathrm{c}}^3E_{\mathrm{sc}}^3\sum_{n=-\infty}^{+\infty}\sum_{p=-\infty}^{+\infty}\sum_{q=-\infty}^{+\infty} J_n(\beta)J_p(\beta)J_q(\beta) \\ &\quad\{\cos\left[2\pi\left((n+p+q)f_{\mathrm{e}}-3\Delta f\right)t\right]\} \\ &= 2\alpha_3E_{\mathrm{c}}^3E_{\mathrm{sc}}^3J_1(3\beta)\cos\left[2\pi\left(f_{\mathrm{e}}-3\Delta f\right)t\right], \end{aligned} \tag{8}$$

which corresponds to the IMD3 directly measured by the electrical spectrum analyzer (ESA). The fraction of the intrinsic PD IMD3 contained in the measured IMD3 can therefore be expressed as:

$$F = \frac{9J_1^6(\beta)}{J_1^2(3\beta)}, \tag{9}$$

where $F$ is the power de-embedding factor. Since $F$ depends on $\beta$, and $\beta$ can be achieved according to the optical power ratio between the first-order sidebands and the carrier from the measured optical spectrum, $F$ can be experimentally obtained. Let $P_1$ and $P_{\mathrm{s}}$ be the optical powers of the +1st-order sideband and the frequency-shifted carrier, respectively, measured by a tap optical power meter (Tap OPM1). The equivalent input optical power $P_{\mathrm{in}}$ is defined as:

$$P_{\mathrm{in}} = \sqrt{P_1P_{\mathrm{s}}}. \tag{10}$$

By sweeping the $P_{\mathrm{in}}$, extracting the powers of the fundamental and IMD3 components, and applying the de-embedding factor, the intrinsic IMD3 can be obtained. Linear fitting yields the input and output third-order intercept points (IIP3 and OIP3). The noise floor consists of shot noise and thermal noise, as expressed by:

$$N_0 = 2qI_{DC}R + kT, \tag{11}$$

where $q$ is the electron charge, $I_{DC}$ is the measured DC photocurrent, $R$ is the load resistance, $k$ is the Boltzmann constant, and $T = 290$ K. The SFDR of the PD is then given by the measured noise floor $N_0$ and the extracted OIP3 as:

$$\mathrm{SFDR} = \frac{2}{3}\left(\mathrm{OIP}_3 - N_0\right). \tag{12}$$

Repeating the above procedure while sweeping the $f_e$ gives the frequency-dependent nonlinear parameters.

The experimental setup is shown in Fig. 1. The optical carrier from Laser 1 (Teraxion, PS-NLL) at 1550.19 nm is split into two paths. In the upper path, the carrier is frequency shifted by 79.75 MHz using AOM1 (G-1550-80) and then phase modulated by a PM (EOSPACE, PM40) driven by an RF signal at frequency $f_e$. In the lower path, the carrier is frequency shifted by 80.25 MHz using AOM2 and delayed by a short fiber to balance the path length mismatch between the two arms. The two paths are recombined to generate a probe signal with a carrier offset of 0.5 MHz. The probe power is swept and monitored by VOA1 (MEMS, VOA-2-1550) and tap OPM1 (GLSUN, TAPD). Laser 2 (Agilent, N7714A) at 1553.05 nm provides the compensation signal, whose power is adjusted by VOA2 and monitored by tap OPM2. The probe signal and the compensation signal are combined to form the excitation signal and then launched into a commercial 70-GHz PD (COHERENT, XPDV3120R). During probe power sweeping, the compensation power is adjusted to maintain a constant total excitation power, thereby stabilizing the PD operating condition. The DC and AC components of the photocurrent are measured by a source meter (Keithley, 2450) and an ESA (R&S, FSW67), respectively.

Figure 2 shows the optical spectra of the phase-modulated signal, the frequency-shifted carrier, and the excitation signal. At $f_e = 40$ GHz and 15 dBm RF drive, the phase-modulated spectrum contains not only the ±1st-order sidebands but also higher-order sidebands owing to the nonlinear response of the PM. These sidebands contribute to the directly measured IMD3 and therefore require de-embedding. The measured power difference between the carrier and the −1st-order sideband is 11.01 dB, corresponding to a phase-modulation index of 0.54 rad and a de-embedding factor of 0.0087 according to Eq. (9). After combining with the compensation signal, the wavelength spacing between Laser 2 and the probe is 357 GHz, far beyond the PD bandwidth. Therefore, the beat terms between the two lasers do not affect the IMD3 measurement. The total excitation optical power is maintained at 9.40 dBm, which is within but close to the specified maximum average optical input power of 10 dBm for the PD under test. During the power sweep from −20.34 dBm to −1.10 dBm, the total excitation power is maintained at 9.40 ± 0.01 dBm, corresponding to a fluctuation range of 9.39–9.41 dBm, while the DC photocurrent remains stable at 5.49 mA.

Figure 3 compares the electrical spectra measured with and without delay balancing. At $f_e = 40$ GHz, and $\Delta f = 0.5$ MHz, two fundamental components at 39.9995 and 40.0005 GHz and the corresponding IMD3 components at 39.9985 and 40.0015 GHz are clearly resolved. Without delay balancing, path mismatch degrades the coherence between the phase-modulated sidebands and the shifted carrier, which introduces frequency-dependent noise and reduces the measurable dynamic range. After delay balancing, the spectral background is significantly suppressed, and the powers of the fundamental and IMD3 components can be extracted more reliably over a wider input power range. The measured fundamental components power differences are 1.41 and 1.47 dB before and after delay balancing, respectively. In the experiment, the optical delay mismatch is first measured to be 28.52 ns using a commercial high-precision optical delay meter (NEWKEPHOTONICS, ODM-S-D) and then compensated by inserting a 5.83-m polarization-maintaining fiber, reducing the residual mismatch to below 34.11 ps.

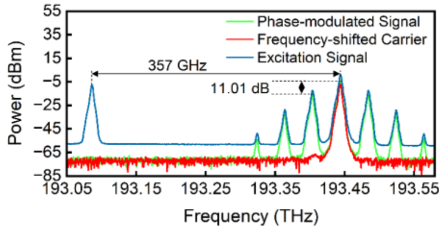


**Fig. 2.** Optical spectra of the phase-modulated signal, frequency-shifted carrier, and excitation signal.

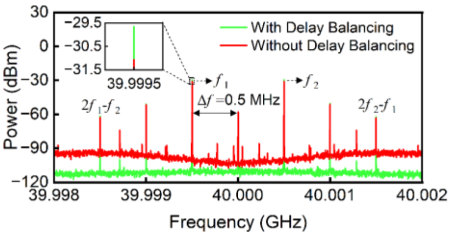


**Fig. 3.** Electrical spectra of the photocurrents generated by the PD under test with and without the delay balancing.

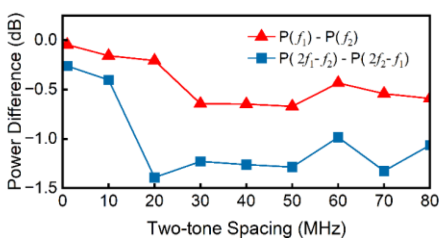


**Fig. 4.** Power differences of the fundamental and IMD3 components under different two-tone frequency spacings.

To minimize the influence of the uneven frequency response of the PD, the two-tone frequency spacing is adjusted by tuning the frequency shifts introduced by AOMs. As shown in Fig. 4, the power difference between the two fundamental components, as well as that between the two IMD3 components, grows due to the frequency response unevenness when the frequency spacing increases from 1 MHz to 20 MHz. For the two-tone frequency spacing exceeding 20 MHz, the power differences between the two fundamental components and between the two IMD3 components are 0.50 and 1.30 dB, respectively. In the following measurement, to minimize the measurement error induced by the uneven linear frequency response, the spacing is set to 1 MHz, for which the corresponding power differences are reduced to about 0.05 and 0.26 dB.

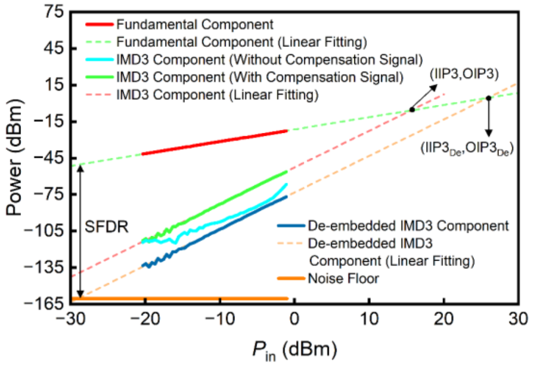


**Fig. 5.** Measured input–output power characteristics of the PD at 40 GHz.

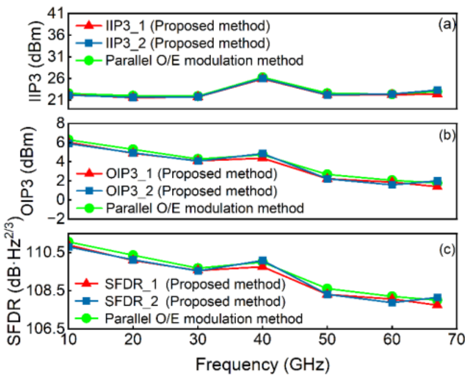


**Fig. 6.** Frequency-dependent third-order nonlinear parameters measurement results for the PD under test.

Figure 5 shows the measured input-output power characteristics at 40 GHz. The $P_{in}$ was swept from −20.34 dBm to −1.10 dBm over 50 points. The measured fundamental power follows the expected slope of 1. The directly measured IMD3 follows the expected slope of 3 only when a compensation signal is applied. Without compensation, the IMD3 curve deviates from the ideal slope and exhibits noticeable fluctuations, confirming that stabilizing the operating point is essential for reliable IMD3 characterization. Applying the de-embedding factor $F = 0.0087$ shifts the IMD3 curve downward substantially, indicating that the directly measured IMD3 is dominated by PM-induced distortion. It should be noted that the RF drive power applied to the PM is kept constant during the power sweeping. Therefore, the modulation index remains unchanged, and the de-embedding factor calculated from Eq. (9) is fixed. Consequently, the de-embedded IMD3 curve is obtained by applying a constant offset to the directly measured IMD3 component. Linear fitting gives IIP3 values before and after de-embedding of 15.60 and 25.90 dBm, respectively, while the corresponding OIP3 values are −5.92 and 4.38 dBm. Throughout the power sweep, the shot-noise level is calculated to be −160.55 dBm/Hz according to Eq. (11), and the thermal-noise level at room temperature is estimated to be −173.98 dBm/Hz. By combining these two contributions in the linear power domain, the total noise floor is obtained as −160.36 dBm/Hz.

Figure 6 shows the frequency-dependent nonlinear parameters. In Figs. 6(a)–6(c), the red and blue curves represent the nonlinear parameters extracted from the two IMD3 components and their corresponding fundamental components, respectively. The IIP3 remains relatively stable over the measured frequency range, whereas the OIP3 decreases with increasing frequency, indicating stronger effective third-order distortion at higher frequencies. According to the manufacturer's frequency response, the PD under test shows a responsivity increase around 40 GHz. This increases the fundamental RF signal power and thus leads to slightly higher IIP3, OIP3, and SFDR at 40 GHz. A similar trend is observed using the parallel O/E modulation method [11]. Since the noise floor shows no obvious frequency dependence over the measured band, the SFDR follows the same trend as the OIP3. To verify the accuracy of the proposed method, the third-order nonlinear parameters of the same PD are also measured using the previously reported parallel O/E modulation method [11]. The results are plotted in Fig. 6 for comparison and show good agreement with those obtained using the proposed method.

In summary, we have demonstrated a method based on improved carrier-shifted phase modulation for accurately characterizing the third-order nonlinear parameters of PD. Optical power compensation is applied during power sweeping to stabilize the PD operating condition and enable stable measurement of the IMD3. By introducing a supplementary optical frequency shifter, the two-tone spacing is reduced to 1 MHz, which minimizes the influence of the uneven PD frequency response. Path length balancing between the phase-modulated signal and the frequency-shifted carrier further suppresses the spectral background, enabling more reliable extraction of the fundamental and IMD3 powers over a wider input power range. After de-embedding the nonlinearity of the PM, the IP3 and SFDR of a commercial PD are accurately measured over 10–67 GHz, confirming the capability of the proposed method for broadband third-order nonlinearity characterization.

**Funding.** National Natural Science Foundation of China (62071226, 62171219).

**Disclosures.** The authors declare no conflicts of interest.

**Data availability.** Data are not publicly available but may be obtained from the authors upon reasonable request.

## REFERENCES

1. L. Wang, X. Wang, and S. Pan, IEEE Trans. Microw. Theory Techn. **73**, 5295 (2025).
2. F. Zhang, J. Li, L. Li, *et al.*, Nat. Commun. **17**, 676 (2025).
3. S. Pan and Y. Zhang, J. Lightwave Technol. **38**, 5450 (2020).
4. Y. Heng, K. Yang, X. Zhu, *et al.*, J. Lightwave Technol. **43**, 10153 (2025).
5. P. Ghelfi, F. Laghezza, F. Scotti, *et al.*, Nature **507**, 341 (2014).
6. X. Xie, K. Li, Q. Zhou, *et al.*, J. Lightwave Technol. **32**, 4187 (2014).
7. D. C. Scott, T. A. Vang, J. Elliott, *et al.*, IEEE Photonics Technol. Lett. **12**, 422 (2000).
8. M. N. Draa, A. S. Hastings, and K. J. Williams, Opt. Express **19**, 12635 (2011).
9. A. Beling, H. Pan, H. Chen, *et al.*, J. Lightwave Technol. **26**, 2373 (2008).
10. N. J. Frigo, M. N. Hutchinson, and J. R. Peasant, J. Lightwave Technol. **34**, 4696 (2016).
11. D. Lei, Y. Xu, X. Zou, *et al.*, Opt. Lett. **49**, 5439 (2024).
12. D. Lei, Y. Xu, X. Zou, *et al.*, Opt. Lett. **50**, 5113 (2025).
13. N. J. Frigo, M. N. Hutchinson, and C. R. S. Williams, J. Lightwave Technol. **36**, 4371 (2018).